

Ultraviolet random lasing from asymmetrically contacted MgZnO metal-semiconductor-metal device

Muhammad M. Morshed, Mohammad Suja, Zheng Zuo, and Jianlin Liu

Citation: *Applied Physics Letters* **105**, 211107 (2014); doi: 10.1063/1.4902921

View online: <http://dx.doi.org/10.1063/1.4902921>

View Table of Contents: <http://scitation.aip.org/content/aip/journal/apl/105/21?ver=pdfcov>

Published by the *AIP Publishing*

Articles you may be interested in

[Energy-selective multichannel ultraviolet photodiodes based on \(Mg,Zn\)O](#)

Appl. Phys. Lett. **103**, 171111 (2013); 10.1063/1.4826596

[The effect of oxygen flow rate and radio frequency plasma power on cubic ZnMgO ultraviolet sensors grown by plasma-enhanced molecular beam epitaxy](#)

Appl. Phys. Lett. **103**, 031114 (2013); 10.1063/1.4815995

[Electrically pumped near-ultraviolet lasing from ZnO/MgO core/shell nanowires](#)

Appl. Phys. Lett. **99**, 063115 (2011); 10.1063/1.3625925

[Electrically pumped ultraviolet random lasing from heterostructures formed by bilayered MgZnO films on silicon](#)

Appl. Phys. Lett. **97**, 061111 (2010); 10.1063/1.3478217

[Ultraviolet photoconductive detector based on epitaxial Mg_{0.34}Zn_{0.66}O thin films](#)

Appl. Phys. Lett. **78**, 2787 (2001); 10.1063/1.1368378



Ultraviolet random lasing from asymmetrically contacted MgZnO metal-semiconductor-metal device

Muhammad M. Morshed, Mohammad Suja, Zheng Zuo, and Jianlin Liu^{a)}

Department of Electrical and Computer Engineering, University of California, Riverside, California 92521, USA

(Received 17 September 2014; accepted 16 November 2014; published online 26 November 2014)

Nitrogen-doped $\text{Mg}_{0.12}\text{Zn}_{0.88}\text{O}$ nanocrystalline thin film was grown on *c*-plane sapphire substrate. Asymmetric Ni/Au and Ti/Au Schottky contacts and symmetric Ni/Au contacts were deposited on the thin film to form metal-semiconductor-metal (MSM) laser devices. Current-voltage, photocurrent, and electroluminescence characterizations were performed. Evident random lasing with a threshold current of ~ 36 mA is demonstrated only from the asymmetric MSM device. Random lasing peaks are mostly distributed between 340 and 360 nm and an output power of 15 nW is measured at 43 mA injection current. The electron affinity difference between the contact metal and $\text{Mg}_{0.12}\text{Zn}_{0.88}\text{O}:\text{N}$ layer plays an important role for electron and hole injection and subsequent stimulated random lasing. © 2014 AIP Publishing LLC.

[<http://dx.doi.org/10.1063/1.4902921>]

Research on developing low-threshold, different-operating-wavelengths, durable, and efficient semiconductor laser diodes over the last several decades has led to intensive material and device engineering, which has introduced GaAs to GaN, and early double heterostructure, through quantum well to plasmonic, random, and nano laser devices.^{1–4} As a direct band gap (3.37 eV) semiconductor along with high exciton binding energy (60 meV, compared to 25 meV of GaN) at room temperature (RT), ZnO has opened up the possibility of very low-threshold, highly efficient excitonic lasing devices at RT.^{5–7} Its alloys, $\text{Mg}_x\text{Zn}_{1-x}\text{O}$ and $\text{Cd}_x\text{Zn}_{1-x}\text{O}$ have added new dimensions to potential applications in deep ultraviolet (UV) and visible spectrum, respectively.^{8,9} Currently, random laser has attracted much attention due to its simplicity in structure and operation process, and potential for various applications such as bio-sensing, medical diagnostic, speckle-free imaging, and information storage.^{10–15} ZnO can be utilized as an excellent random lasing medium due to its high refractive index and exciton binding energy. However, lack of reliable p-type ZnO is the bottleneck problem toward achieving high-performance ZnO based light emitting devices, even though ZnO-based homojunctions, mostly LED devices have been reported.^{16–20} Hence, ZnO thin film based alternative random lasing device structures such as metal-insulator-semiconductor (MIS) structures, heterostructured devices with the combination of n-ZnO and other p-type materials have drawn a great deal of interest.^{21–25}

In this letter, random lasing from an asymmetrically contacted metal-semiconductor-metal (MSM) device is reported. The device consists of Ni/Au and Ti/Au Schottky contacts to N-doped $\text{Mg}_{0.12}\text{Zn}_{0.88}\text{O}$ nanocrystalline thin film grown by RF plasma-assisted molecular beam epitaxy. N doping and Mg alloying effectively reduce the carrier concentration in the semiconductor, which enhances diffusion of

holes from Ni/Au/MgZnO Schottky contact to recombine with electrons from Ti/Au/MgZnO contact. Light propagates through the nanocrystalline thin film and subjects to multiple scattering, leading to random lasing. The demonstration of random lasing from MSM device suggests that even very limited hole supply as a result of leakage current from a reverse-biased metal semiconductor junction in the MSM structure is sufficient to recombine with electrons to initiate random lasing in ZnO based materials. Therefore, excitonic processes have played an important role in ZnO random lasing.

First, a MgO/ZnO bi-layer of 15 nm was deposited at 450 °C as the nucleation layer on a cleaned *c*-plane sapphire substrate. On top of this nucleation layer, a ZnO (400 nm) buffer film was deposited at a substrate temperature of 500 °C, a Zn cell temperature of 350 °C, an oxygen (O_2) flow of 3 sccm, and a plasma power of 400 W. Next, N-doped $\text{Mg}_{0.12}\text{Zn}_{0.88}\text{O}$ (250 nm) was deposited at the same substrate temperature with Zn, Mg cell temperature, and $\text{O}_2/\text{N}_2\text{O}$ flow at 346 °C, 435 °C, and 2.5/2.5 sccm, respectively. After the growth, the sample was *in situ* annealed at 600 °C for 20 min with 3 sccm of O_2 flow. This film, initially exhibiting p-type behavior,²⁶ is converted to n-type over a period of time with a high resistivity ($\sim 10^2 \Omega\text{-cm}$).

Circular geometry ($\sim 400 \mu\text{m}$ outside diameter) planar MSM device structure was fabricated following the standard photolithography process. Ni/Au (20 nm/150 nm) and Ti/Au (20 nm/150 nm) were deposited on the surface of $\text{Mg}_{0.12}\text{Zn}_{0.88}\text{O}:\text{N}$ layer as the inner and outer concentric circular contact metals, respectively, for the asymmetric MSM device. For the symmetric MSM device, Ni/Au (20 nm/150 nm) was used for both contacts. Current–voltage (*I*–*V*) characteristic of the device was measured using an Agilent 4155C semiconductor parameter analyzer. Photoluminescence (PL) and electroluminescence (EL) measurements were carried out using a PL/EL system composed of an Oriel monochromator, a photomultiplier detector, a lock-in amplifier, and a chopper. A 325-nm wavelength (Kimmon) He–Cd laser was used as an

^{a)} Author to whom correspondence should be addressed. Electronic mail: jianlin@ee.ucr.edu.

excitation source for PL measurement. An external HP E3630A dc power supply was used to input current for EL measurements. Photocurrent (PC) measurement was carried out using a 150 W Xe arc lamp as light source. The devices were packaged on TO5 Cans for EL and PC measurements. Output power of the device was measured using a Thorlabs PM100 optical power meter.

Figure 1(a) shows x-ray diffraction (XRD) pattern of the $\text{Mg}_{0.12}\text{Zn}_{0.88}\text{O:N}$ film. The peak at $\sim 34.4^\circ$ indicates preferential growth along the c -direction of the wurtzite lattice structure, according to the standard card (JCPDS 36-1451). The top and bottom right insets in Fig. 1(a) show top and cross sectional scanning electron microscopy (SEM) images of the film, respectively. The film exhibits nanoscale columnar structures with many pits or air gaps in between. This morphology originates from the low-quality MgO/ZnO buffer and subsequent growth of large lattice mismatched active layer with respect to the substrate at relatively low temperature.¹¹ Figure 1(b) shows RT PL spectrum of the $\text{Mg}_{0.12}\text{Zn}_{0.88}\text{O:N}$ film. The excitonic near band edge peak is around 355 nm (3.49 eV) and deep level emissions are

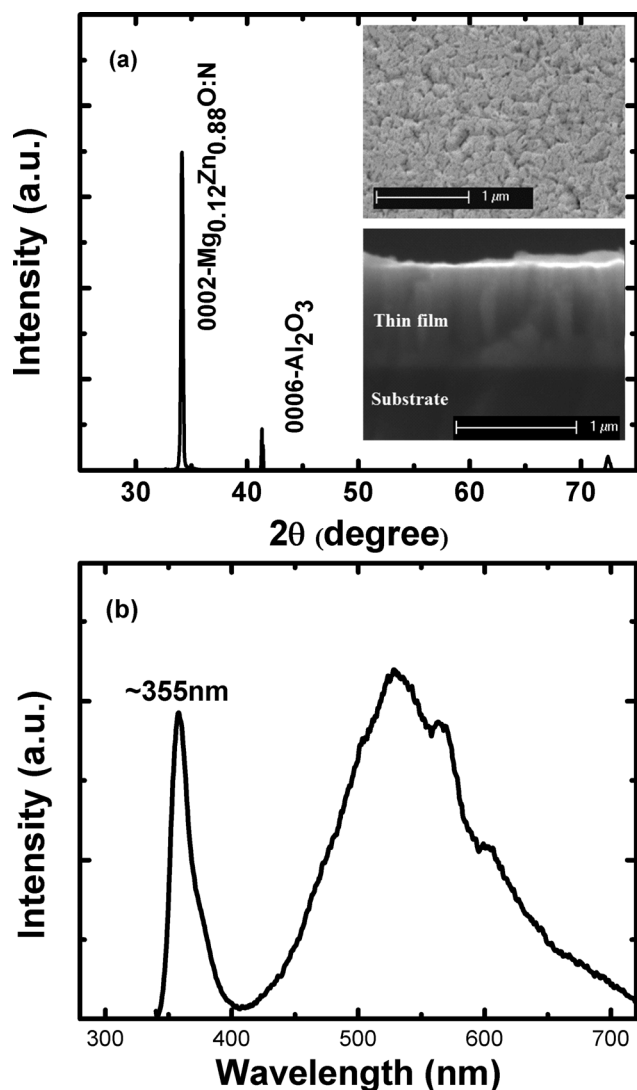


FIG. 1. (a) XRD pattern of the $\text{Mg}_{0.12}\text{Zn}_{0.88}\text{O:N}$ film. The top and bottom right insets show SEM images of the top surface and cross sectional view, respectively. (b) RT photoluminescence spectrum of the $\text{Mg}_{0.12}\text{Zn}_{0.88}\text{O:N}$ film.

present in the spectrum. These interband states are mainly due to the point defects (interstitials, vacancies, anti-sites, etc.) in the film formed under O-rich growth condition.^{27,28}

Figure 2 shows I-V characteristics of the asymmetric MSM device with and without UV illumination. The bottom right inset shows I-V characteristics of the symmetric MSM device and top left inset shows top-view schematic of the device structure. The I-V curves exhibit almost symmetric behavior under forward (positive voltage on Ni/Au contact) and reverse biases, which are a typical characteristic of MSM device.^{29,30} However, the dark current is less under reverse bias for the asymmetric MSM device, as the electrons overcome higher energy barrier at the Ni contact junction, compared to the barrier at Ti contact junction under forward bias. Both devices show enhanced photoresponses under UV exposure indicating resistive nature of the N-doped $\text{Mg}_{0.12}\text{Zn}_{0.88}\text{O}$ film, where the photo-generated carriers contribute to increased conductivity.³⁰

Figure 3(a) shows PC spectra under zero and forward (positive voltage on the Ni/Au contact) biases for the asymmetric MSM device. The inset shows PC spectra under reverse (positive voltage on the Ti/Au contact) bias. With zero bias, the photocurrent is absent due to Schottky barriers to the photo-generated carriers.³⁰ Under both forward and reverse biases, the photocurrent response increases as the photo-generated carriers are swept and collected under the applied electric field. The spectra show a peak at around 350–360 nm as the carriers are generated within the $\text{Mg}_{0.12}\text{Zn}_{0.88}\text{O:N}$ layer. Figure 3(b) shows PC spectra under different applied voltages for the symmetric MSM device. The spectra show similar trend as the asymmetric MSM device. Long tail response is observed on the lower energy side of the spectra, which is due to carrier generation from the intraband states within the film. This enhanced photocurrent response is a result of more efficient collection of electrons and holes from the N-doped $\text{Mg}_{0.12}\text{Zn}_{0.88}\text{O}$ film at higher voltages.³¹

Figure 4(a) shows EL spectra with continuous dc current injection (through Ni/Au contact to Ti/Au contact) at room temperature from the asymmetric MSM device. The EL was recorded from the normal direction of the sample surface. At low current injection (33–35 mA), the emission is broad and

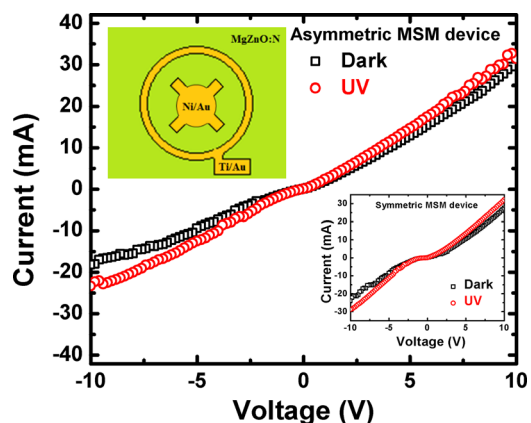


FIG. 2. I-V characteristic in linear scale of the asymmetric MSM device under UV and dark. The top left inset shows top-view schematic of the device structure. The bottom right inset shows the I-V characteristic of the symmetric MSM device.

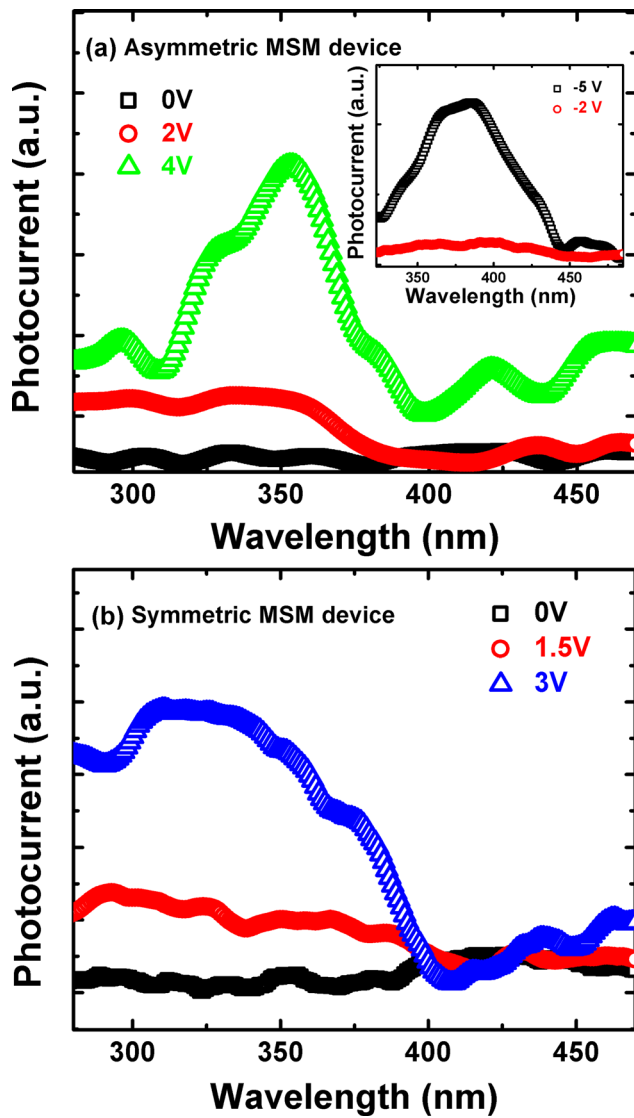


FIG. 3. (a) Photocurrent spectra under different biases (positive voltage on Ni/Au contact) from the asymmetric MSM device. The top right inset shows the photocurrent spectra under reverse (positive voltage on Ti/Au contact) bias. (b) Photocurrent spectra under different biases from the symmetric MSM device.

weak for the asymmetric MSM device. With higher current injection (>35 mA), multiple emission peaks appear. The peaks are distributed mostly between 340 and 360 nm. The intensity becomes stronger with increasing injection current and also the line width gets narrower (~ 2 – 3.5 nm). On the other hand, the emission from the symmetric MSM device as shown in the inset spectra is broad and weak, and multiple emission peaks with line width narrowing trend at higher injection current are absent. Figure 4(b) shows EL spectra at different detection angle under 43 mA current injection for the asymmetric MSM device. Different peaks appear at varying angle of measurement and the spacing between adjacent peaks also varies with each measurement. The increasing intensity, line width narrowing of multiple peaks with higher injection current and inhomogeneous distribution of peaks at different angle of measurement suggest random lasing from the asymmetric MSM device.^{32,33} Figure 4(c) shows integrated light intensity as a function of injection current for the asymmetric MSM device. A threshold current of around

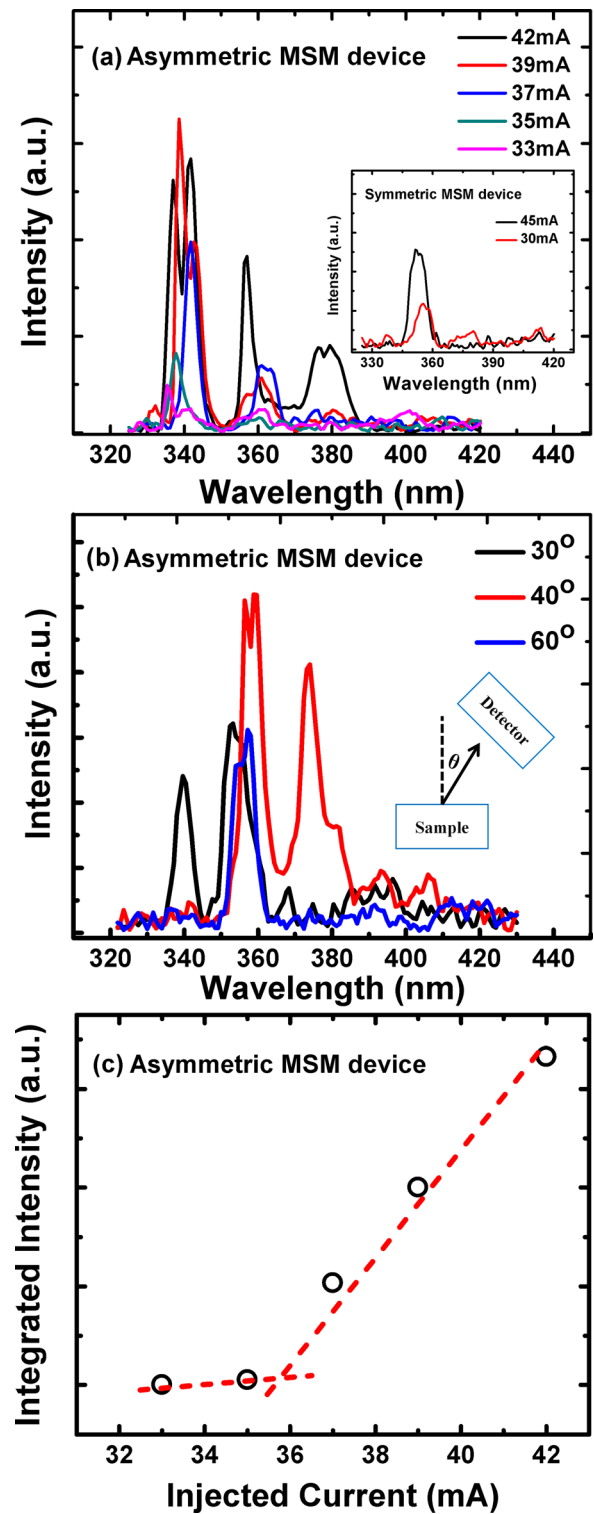


FIG. 4. (a) RT EL spectra under different injection current from the asymmetric MSM device. The bottom right inset shows EL spectra from the symmetric MSM device. (b) Angle-dependent EL spectra at an injection current of 42 mA, and (c) integrated EL intensity at different injection current of the asymmetric MSM device.

~ 36 mA is evident. Light output power of ~ 15 nW was detected at 43 mA injection current. The necessary cavity for the lasing is formed randomly through light scattering at the column boundaries with air gaps inside the film.¹¹ However, weak confinement of light and spatial overlapping of random cavity modes with large cavity length, which depends on the density of scattering centers, lead to random diffusing of

photons from neighboring cavities and mode coupling, and interrupting the coherence of the cavity mode. These disruptions in the cavity cause broad line width of the lasing modes.^{34,35} In contrast, narrow line widths of less than 0.2 nm can be achieved in the devices comprising of more loosely packed ZnO columnar structures or bundle nanowires.^{16,22}

Finally, we briefly discuss the lasing mechanism of the asymmetric MSM device. Under applied positive voltage on Ni/Au contact in the asymmetric MSM device, electrons can easily overcome the shallower Ti contact barrier through thermionic emission. At higher voltage, much of the voltage is dropped across the thin film and Ni/MgZnO Schottky diode regions, which leads to more energy band bending compared to that of the Ti contact region. Hence, holes can tunnel directly and also through traps to the valence band of $\text{Mg}_{0.12}\text{Zn}_{0.88}\text{O:N}$ film from the Ni contact across the sharply bent energy band region.^{36,37} Moreover, some holes are created through the generation process due to the presence of high electric field near the Ni-contact region. These injected holes readily form excitons and contribute to the excitonic electroluminescence. However, due to limited number of holes or excitons, the gain of the active medium is small, leading to low emission intensity and output power. Compared with asymmetric MSM device, the symmetric MSM device adopts both Ni/Au metal contacts, which have larger Schottky barrier height than the Ti/Au contact. Under similar operation condition to the asymmetric MSM device, much less holes are injected into the thin film region in the symmetric MSM device, therefore, very weak EL is observed.

Electrically pumped random lasing is observed from $\text{Mg}_{0.12}\text{Zn}_{0.88}\text{O:N}$ thin film based asymmetric MSM device. I-V and photocurrent characteristics show typical MSM device characteristics from the resistive $\text{Mg}_{0.12}\text{Zn}_{0.88}\text{O:N}$ layer. The electron affinity of the contact metals affects the efficiency of hole injection. Column morphology of the thin film with air gaps provides the scattering media to form random cavity. A threshold current of ~ 36 mA is observed and an output power of ~ 15 nW is obtained at a drive current of 43 mA. This work shows an alternative approach for $\text{Mg}_x\text{Zn}_{1-x}\text{O}$ based random lasing device and opens up the opportunity to achieve random lasers towards deep UV wavelengths with a simple device structure.

The authors acknowledge the financial support from the Department of Energy (DE-FG02-08ER-46520).

¹Z. I. Alferov, *Semiconductors* **32**, 1 (1998).

²S. Nakamura, M. Senoh, S. Nagahama, N. Iwasa, T. Yamada, T. Matsushita, H. Kiyoku, and Y. Sugimoto, *Jpn. J. Appl. Phys., Part 2* **35**, L74 (1996).

- ³R. F. Oulton, V. J. Sorger, T. Zentgraf, R. Ma, C. Gladden, L. Dai, G. Bartal, and X. Zhang, *Nature* **461**, 629 (2009).
- ⁴M. A. Noginov, G. Zhu, A. M. Belgrave, R. Bakker, V. M. Shalaev, E. E. Narimanov, S. Stout, E. Herz, T. Suteewong, and U. Wiesner, *Nature* **460**, 1110 (2009).
- ⁵D. M. Bagnall, Y. F. Chen, Z. Zhu, T. Yao, S. Koyama, M. Y. Shen, and T. Goto, *Appl. Phys. Lett.* **70**, 2230 (1997).
- ⁶S. Chu, G. Wang, W. Zhou, Y. Lin, L. Chernyak, J. Zhao, J. Kong, L. Li, J. Ren, and J. Liu, *Nat. Nanotechnol.* **6**, 506 (2011).
- ⁷S. F. Yu, C. Yuen, S. P. Lau, W. I. Park, and G. C. Yi, *Appl. Phys. Lett.* **84**, 3241 (2004).
- ⁸T. Makino, Y. Segawa, M. Kawasaki, A. Ohtomo, R. Shiroki, K. Tamura, T. Yasuda, and H. Koinuma, *Appl. Phys. Lett.* **78**, 1237 (2001).
- ⁹T. Takagi, H. Tanaka, S. Fujita, and S. Fujita, *Jpn. J. Appl. Phys., Part 2* **42**, L401 (2003).
- ¹⁰S. Chu, M. Olmedo, Z. Yang, J. Kong, and J. Liu, *Appl. Phys. Lett.* **93**, 181106 (2008).
- ¹¹J. Kong, S. Chu, Z. Zuo, J. Ren, M. Olmedo, and J. Liu, *Appl. Phys. A* **107**, 971 (2012).
- ¹²D. S. Wiersma and A. Lagendijk, *Phys. Rev. E* **54**, 4256 (1996).
- ¹³D. S. Wiersma, *Nat. Phys.* **4**, 359 (2008).
- ¹⁴Q. Song, S. Xiao, Z. Xu, V. M. Shalaev, and Y. L. Kim, *Opt. Lett.* **35**, 2624 (2010).
- ¹⁵B. Redding, M. A. Choma, and H. Cao, *Nat. Photonics* **6**, 355 (2012).
- ¹⁶S. Chu, J. H. Lim, L. J. Mandalapu, Z. Yang, L. Li, and J. Liu, *Appl. Phys. Lett.* **92**, 152103 (2008).
- ¹⁷J. C. Sun, J. Z. Zhao, H. W. Liang, J. M. Bian, L. Z. Hu, H. Q. Zhang, X. P. Liang, W. F. Liu, and G. T. Du, *Appl. Phys. Lett.* **90**, 121128 (2007).
- ¹⁸K. Nakahara, S. Akasaka, H. Yuji, K. Tamura, T. Fujii, Y. Nishimoto, D. Takamizu, A. Sasaki, T. Tanabe, H. Takasu, H. Amaike, T. Onuma, S. F. Chichibu, A. Tsukazaki, A. Ohtomo, and M. Kawasaki, *Appl. Phys. Lett.* **97**, 013501 (2010).
- ¹⁹W. F. Liu, J. M. Bian, L. Z. Hu, H. W. Liang, H. Q. Zang, J. C. Sun, Z. W. Zhao, A. M. Liu, and G. T. Du, *Solid State Commun.* **142**, 655 (2007).
- ²⁰H. Kato, T. Yamamuro, A. Ogawa, C. Kyotani, and M. Sano, *Appl. Phys. Express* **4**, 091105 (2011).
- ²¹Y. Tian, X. Ma, P. Chen, Y. Zhang, and D. Yang, *Opt. Express* **18**, 10668 (2010).
- ²²X. Ma, J. Pan, P. Chen, D. Li, H. Zhang, Y. Yang, and D. Yang, *Opt. Express* **17**, 14426 (2009).
- ²³H. K. Liang, S. F. Yu, and H. Y. Yang, *Appl. Phys. Lett.* **96**, 101116 (2010).
- ²⁴E. S. P. Leong and S. F. Yu, *Adv. Mater.* **18**, 1685 (2006).
- ²⁵H. Long, G. Fang, S. Li, X. Mo, H. Wang, H. Huang, Q. Jiang, J. Wang, and X. Zhao, *IEEE Electron Device Lett.* **32**, 54 (2011).
- ²⁶M. M. Morshed, Z. Zuo, J. Huang, J. Zheng, Q. Lin, X. Yan, and J. Liu, *Appl. Phys. A* **117**, 1467 (2014).
- ²⁷A. Janotti and C. G. Van de Walle, *Phys. Rev. B* **76**, 165202 (2007).
- ²⁸J. Lv and C. Li, *Appl. Phys. Lett.* **103**, 232114 (2013).
- ²⁹L. J. Mandalapu, F. X. Xiu, Z. Yang, and J. L. Liu, *J. Appl. Phys.* **102**, 023716 (2007).
- ³⁰K. Liu, M. Sakurai, and M. Aono, *Sensors* **10**, 8604 (2010).
- ³¹H. L. Porter, A. L. Cai, J. F. Muth, and J. Narayan, *Appl. Phys. Lett.* **86**, 211918 (2005).
- ³²M. Kawasaki, A. Ohtomo, I. Ohkubo, H. Koinuma, Z. K. Tang, P. Yu, G. K. L. Wang, B. P. Zhang, and Y. Segawa, *Mater. Sci. Eng., B* **56**, 239 (1998).
- ³³H. Cao, *Waves Random Med.* **13**, R1 (2003).
- ³⁴L. Florescu and S. John, *Phys. Rev. Lett.* **93**, 013602 (2004).
- ³⁵J. Liu, P. D. Garcia, S. Ek, N. Gregersen, T. Suhr, M. Schubert, J. Mørk, S. Stobbe, and P. Lodahl, *Nat. Nanotechnol.* **9**, 285 (2014).
- ³⁶C. H. Lin and C. W. Liu, *Sensors* **10**, 8797 (2010).
- ³⁷P. G. Kasherinov, A. V. Kichaev, and A. A. Tomasov, *Semiconductors* **29**, 1092 (1995), e-print [arXiv:0704.2703](https://arxiv.org/abs/0704.2703).